Materials Letters 323 (2022) 132570

Contents lists available at ScienceDirect

Materials Letters

journal homepage: www.elsevier.com/locate/matlet

Enhanced heterogeneous nucleation of $Al_6(Fe,Mn)$ compound in Al alloys by interfacial segregation of Mn on TiB_2 particles surface

Zhongping Que [a,*], Yun Wang [a], Zhongyun Fan [a], Teruo Hashimoto [b], Xiaorong Zhou [b]

[a] Brunel Centre for Advanced Solidification Technology (BCAST), Brunel University London, Uxbridge, Middlesex UB8 3PH, UK
[b] School of Materials, University of Manchester, Manchester M13 9PL, UK

ARTICLE INFO

Keywords:
Heterogeneous nucleation
Grain refiner
$Al_6(Fe,Mn)$
Interfacial segregation
Al alloys

ABSTRACT

In this study, the composition templating theory for heterogeneous nucleation was applied to achieve TiB_2 particles with Mn segregation on the surface, which supplied the initial composition for the heterogeneous nucleation. The interfacial segregation of added alloy element Mn and the other common impurities, such as Fe and Si, was investigated with scanning transmission electron microscopy (STEM). The modified TiB_2 particles was applied in Al-2.0Mn-1.0Fe alloys to test its effects on grain refinement of $Al_6(Fe,Mn)$ compound. The interfaces between $Al_6(Fe,Mn)$ particles and the engulfed TiB_2 particles were examined with TEM observation.

1. Introduction

As one of the big challenges to improve the mechanical properties of recycled Al alloys, the controlling of Fe-rich intermetallic compounds (FIMCs) attracted extensive attentions [1]. Understanding of the formation mechanism of IMCs is of priority and significance before any effective approach can be taken to modify or refine them. More than 20 kinds of FIMCs were reported in Al alloys until now, such as α-AlFeSi, $Al_6(Fe,Mn)$ [2–3]. These FIMCs have different crystal structures, different compositions, and different morphologies from each other, and they are easy to form together during the nucleation selection and phase transformation [4].

$Al_6(Fe,Mn)$ phase which has orthorhombic crystal structure, with its lattice parameters being: a = 7.498 Å, b = 6.495 Å, and c = 8.837 Å, [3] was reported to be of a hollow needle-like morphology. IMCs particles with needle- or plate-like morphology are extremely harmful for the mechanical properties, especially the ductility of Al alloys. Therefore, effective refinement of these FIMCs is of both scientific and technological importance. Enhancing heterogeneous nucleation during solidification process is the ideal way to refine the FIMCs.

Our research group being focused on the fundamentals of the heterogenous nucleation and the grain refinement of FIMCs in Al alloys recent years. The latest understanding demonstrates that heterogeneous nucleation of IMCs is difficult and therefore requires large nucleation undercooling [5]. It shows that the undercooling required for heterogeneous nucleation of IMCs is in the order of tens of Kelvin, and that the undercooling increases with increasing complexity of the stoichiometry of the IMCs. This is because nucleation of IMCs needs to create nuclei which have not only the correct crystal structure but also the correct elemental compositions. In this work, we developed a new approach to enhancing heterogeneous nucleation of IMCs by providing both structural templating and compositional templating.

2. Experimental

In this study, the TiB_2 particles were synthesised in an Al-3.7Ti-1.5B-1Mn master alloy which was prepared by melting commercial purity aluminium (CP-Al, >99.86 wt% Al) (all compositions in this paper are in wt.% unless specified otherwise) at 800 °C, followed by addition of Al-10Ti and Al-5B master alloys. The Al-20% Mn master alloy was last added into the melt. The melt was finally casted into thin plates in a steel mould.

Refinement of $Al_6(Fe,Mn)$ compound with modified TiB_2 particles was studied in an Al-2Mn-1Fe alloy which has a composition of 2.2 ± 0.2 Mn, 1.0 ± 0.2 Fe and balanced Al. This alloy was prepared at 750 °C with CP-Al, Al-20Mn and Al-45Fe master alloys. The prepared alloy melt was separated into two equal amounts for the casting without and with 1000 ppm (0.1 %) modified Al-3.7Ti-1.5B master alloy. The standard TP-1 test [6] was used to assess the solidified microstructure of the alloy. At 680 °C, the melts were poured separately into the TP-1 mould which had preheated to 380 °C.

The solidification microstructure was examined using a Zeiss field

* Corresponding author.
E-mail address: Zhongping.Que@brunel.ac.uk (Z. Que).

https://doi.org/10.1016/j.matlet.2022.132570
Received 17 May 2022; Received in revised form 30 May 2022; Accepted 1 June 2022
Available online 3 June 2022

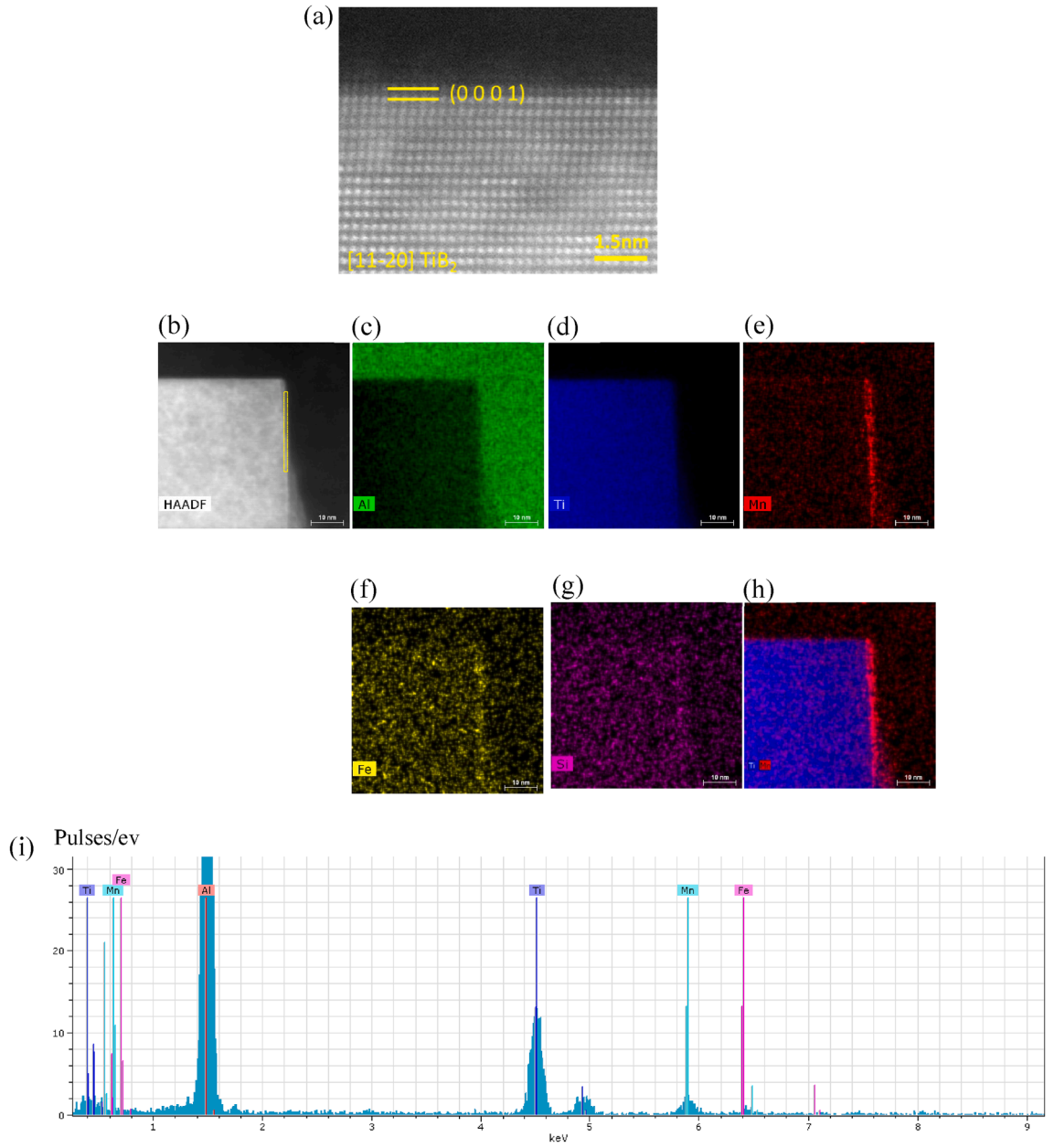

Fig. 1. (a) and (b) STEM Z-contrast HAADF image of Al/TiB_2 interface in Al-3.7Ti-1.5B alloy, viewed along [11$\bar{2}$0] TiB_2 direction, (c-i) Super-X EDS elemental mapping of (b), (c) Al, (d) Ti, (e) Mn, (f) Fe, (g) Si, (h) Ti + Mn overlap image showing the Mn segregation, and (i) super-X EDS spectrum taken from the local region marked in (b) at the interface.

emission gun (FEG) Supera 35 scanning electron microscope (SEM) operated at an accelerating voltage of 5–20 kV. To investigate the 3-dimension(3D) morphology of the IMCs, samples were etched in an etchant of an aqueous solution containing 15 vol% HCl for 1–3 min, followed by a completely but gently cleaning in an ethanol bath. The TEM examination was performed on a JEOL 2100F microscope equipped with EDS facility operated at an accelerating voltage of 200 kV. Atomic resolution STEM with Z-contrast high-angle annular dark-field (HAADF) imaging was carried out on an aberration (Cs)-corrected FEI Titan 80–200 instrument equipped with Super-X energy dispersive X-ray spectroscopy (Super-X EDS) system, operated with an accelerating voltage of 200 kV. High-resolution elemental mapping by STEM/Super-X EDS was also conducted to obtain compositional profiles.

3. Results and discussion

Fig. 1 shows the HAADF STEM image and the corresponding Super-X EDS elemental mapping across the TiB_2/Al interface in Al-3.7Ti-1.5B-1Mn master alloy. The EDS mapping results, Fig. 1(c-h), show a very clear and strong segregation of Mn on the (0 0 0 1) plane of TiB_2 particle. The overlapping mapping results of Ti and Mn, Fig. 1h, shows that the Mn segregation is on the surface of (0 0 0 1) of TiB_2 particles. A very weak segregation signal of Mn is also detected at Al/(1 0 –1 0)TiB_2 interface from the mapping (Fig. 1e). Other alloy elements exist in Al alloys as the common impurities, such as Fe and Si. Their segregation on the TiB_2 particles in this study were also investigated. The mapping results (Fig. 1f and g) show that no Si segregates on the TiB_2 particles surface under this experimental condition, but a very weak Fe segregation signal is detected at α-Al/(0 0 0 1)TiB_2 interface (Fig. 1f). The obvious Mn peak shown in the super-X EDS spectrum (Fig. 1i) taken from the local region

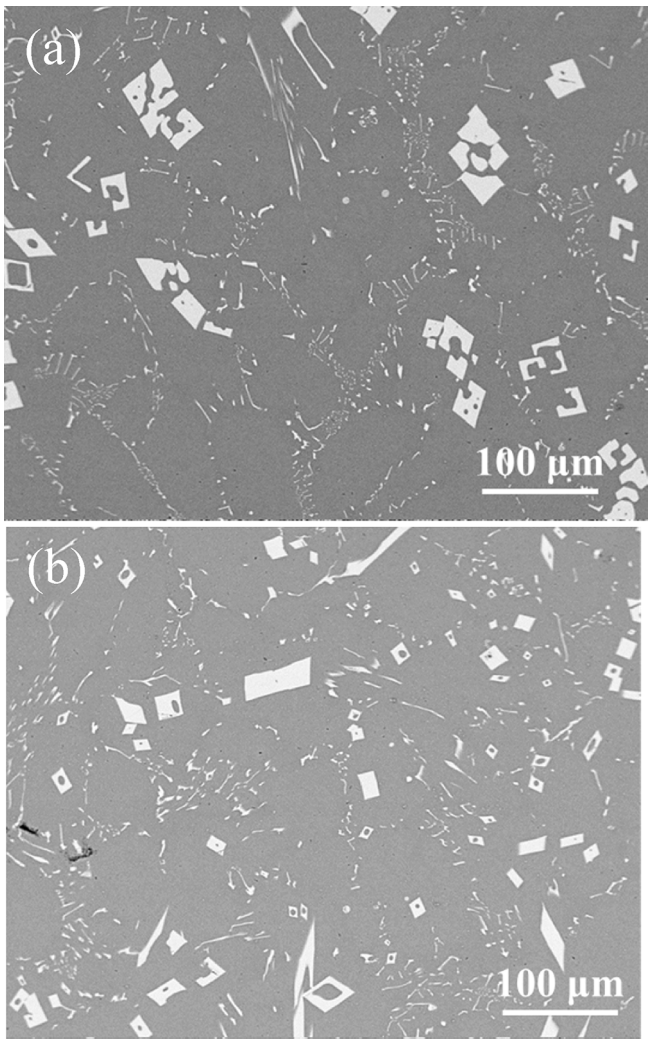

Fig. 2. SEM images showing the microstructure of Al-2Mn-1.0Fe alloy solidified at 3.5 K/s (a) without grain refiner addition, and (b) with 1000 ppm novel grain refiner addition.

marked in (b) at the interface also demonstrates a obvious peak signal of Mn and a weak peak signal of Fe at α-Al/(0001)TiB_2 interface. It demonstrates that the Fe can segregate on TiB_2 surface at impurity concentration.

Although the interfacial segregation of Mn and Fe are very clear, the HAADF image (Fig. 1a) shows no obviously abnormal atomic arrangement on the top of the (0001) TiB_2 surface. This indicates that no in-plane ordered 2-dimension compound was resulted from the interfacial segregation of Mn and Fe at the α-Al/(0001)TiB_2 interface.

The casting microstructures of the Al-2.0Mn-1.0Fe alloy solidified at 3.5 K/s without and with modified TiB_2 particles were shown in Fig. 2. The microstructures of the Al-2.0Mn-1.0Fe alloy are consists of the primary(P-) Al_6(Fe,Mn) with hollow rhombic morphology, some α-Al and binary eutectic (BE-) (Al_6(Fe,Mn) + α-Al) with Chinese script morphology. Due to the difficulty to measure the length for the long needle-like compounds, the sizes of the cross section of compound particles were measured to show the variation before and after grain refiner addition. The longest sides on the cross sections of more than 100 Al_6(Fe,Mn) particles were measured. The average length (Lo) of the rhombic P-Al_6(Fe,Mn) particles in Al-2.0Mn-1.0Fe without grain refiner addition was measured as 26.0 ± 2.1 μm. Fig. 2b shows that the size of P-Al_6(Fe,Mn) is reduced and the number of P-Al_6(Fe,Mn) particles is increased obviously.

The Lo was measured as 9.5 ± 0.6 μm, compared to 26.0 ± 2.1 μm with no addition of the grain refiner. Fig. 2b also shows that the grain boundaries were partially wetted by the formation of the BE-(Al_6(Fe, Mn) + α-Al), which was expected to strongly influence the overall mechanical properties [7].

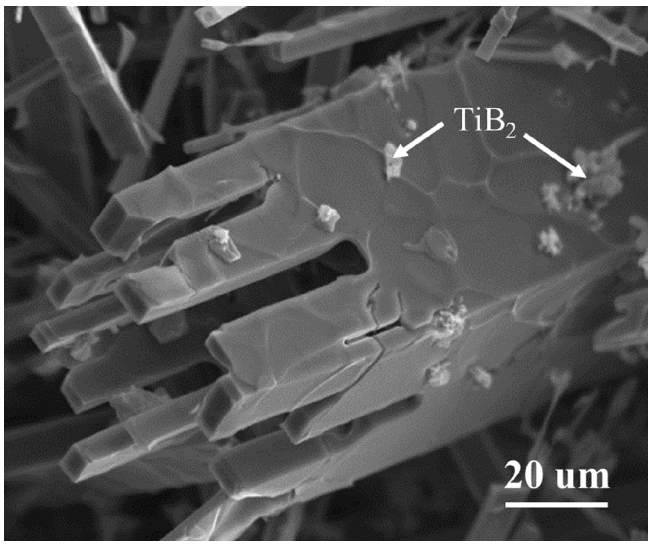

Fig. 3. 3D morphology of primary Al_6(Fe,Mn) in Al-2Mn-1.0 Fe alloy with grain refiner addition solidified at 3.5 K/s.

The 3D morphology of P-Al_6(Fe,Mn) phase in Al-2.0Mn-1.0Fe alloy with grain refiner addition is shown in Fig. 3. The hollow morphology of the primary Al_6(Fe,Mn) particle and the tip of the particle with a few faceted branches are clearly seen. A few TiB_2 particles were observed to be engulfed in these Al_6(Fe,Mn) particles.

TEM observation at the interface between the modified TiB_2 and Al_6(Fe,Mn) particles shows that although most of the engulfed TiB_2 particles have no specifically orientation relationship (OR) with the Al_6(Fe,Mn) particles, a well-defined OR between some TiB_2 particles and Al_6(Fe,Mn) can be observed. The TEM bright field image in Fig. 4a shows a TiB_2 particle embedded in Al_6(Fe,Mn). Selected area electron diffraction (SAED) pattern in Fig. 4b was taken from both the TiB_2 particle and the adjacent Al_6(Fe,Mn) with the incident electron beam being paralleled to both [021] Al_6(Fe,Mn) and [11–20] TiB_2 zone direction. The indexed diffraction pattern in Fig. 4c suggests an orientation relationship (OR) between Al_6(Fe,Mn) and TiB_2: (200) Al_6(Fe,Mn) ~ (0001) TiB_2 and [021] Al_6(Fe,Mn) // [11–20] TiB_2. The [021] zone direction of Al_6(Fe,Mn) has a small deviation of −0.4° in α, and −2.2° in β direction from the zone direction of TiB_2 [11–20]. It means that a small twist by 2.2° angle is between the two zone directions of TiB_2 and Al_6(Fe, Mn). Or in other words, the actual zone direction of Al_6(Fe,Mn) paralleled to [11–20] zone direction of TiB_2 is a high indexed zone direction. In the HRTEM image, Fig. 4d, the incident electron beam is parallel to the [021] zone direction of Al_6(Fe,Mn) (upper part) and with a small angle of 2.2° from the [11–20] TiB_2 (lower part). The observation of the OR provides a direct evidence to confirm that the modified TiB_2 particles do nucleate Al_6(Fe,Mn).

4. Conclusions

Interfacial segregation of elements such as Mn, Fe and Si on TiB_2 surface in Al-3.7Ti-1.5B alloy was investigated. Mn as the added alloy element and Fe at impurity content were found to segregate at the α-Al/(0 0 0 1)TiB_2 interface. However, the interfacial segregation of Fe is weaker than that of Mn. No segregation of Si at impurity concentration was observed at the TiB_2 surface in this study. The size of P-Al_6(Fe,Mn) in Al-2.0Mn-1.0Fe alloy was reduced from 26.0 ± 2.1 μm to 9.5 ± 0.6 μm after addition of 1000 ppm of the Al-3.7Ti-1.5B grain refiner. An OR

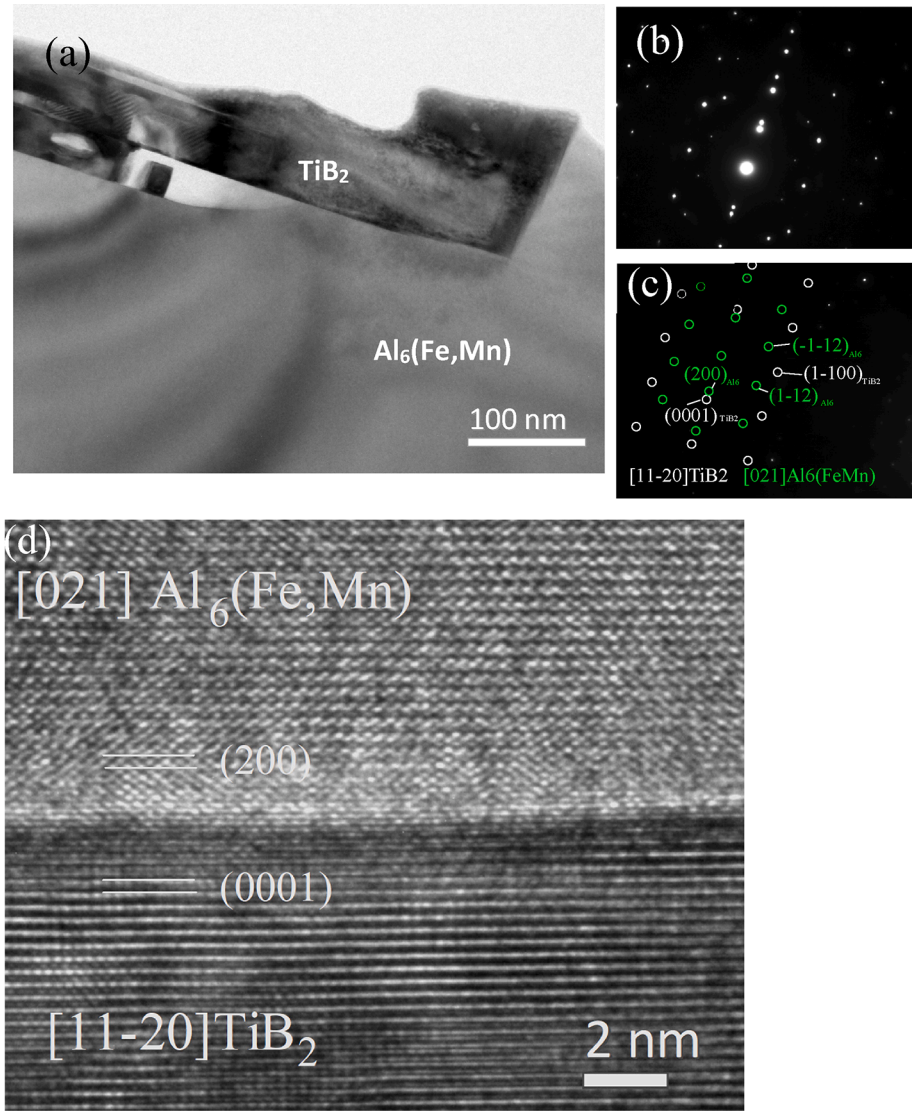

Fig. 4. (a) TEM bright field image showing the $TiB_2/Al_6(Fe,Mn)$ interface, (b) and (c) corresponding selected area electron diffraction (SAED) pattern and indexed pattern taken from both the TiB_2 and adjacent $Al_6(Fe,Mn)$, (d) high resolution TEM (HRTEM) image showing the modified $TiB_2/Al_6(Fe,Mn)$ interface.

between $Al_6(Fe,Mn)$ and TiB_2 was defined: (2 0 0) $Al_6(Fe,Mn)$ ~ (0 0 0 1) TiB_2 and [0 2 1] $Al_6(Fe,Mn)$ //2.2° [1 1 –2 0] TiB_2 was defined.

CRediT authorship contribution statement

Zhongping Que: Conceptualization, Methodology, Investigation, Data curation, Writing – original draft, Writing – review & editing. **Yun Wang:** Investigation, Writing – review & editing. **Zhongyun Fan:** Supervision, Funding acquisition. **Teruo Hashimoto:** Investigation. **Xiaorong Zhou:** Resources.

Declaration of Competing Interest

The authors declare the following financial interests/personal relationships which may be considered as potential competing interests: ZHONGYUN FAN reports financial support was provided by Engineering and Physical Sciences Research Council.

Acknowledgement

The EPSRC is gratefully acknowledged for providing financial support under Grant EP/H026177/1.

References

[1] T.O. Mbuya, B.O. Odera, S.P. Ng'ang'a, Influence of iron on castability and properties of aluminium silicon alloys: literature review, Int. J. Cast Met. Res. 16 (5) (2003) 451–465, https://doi.org/10.1080/13640461.2003.11819622.
[2] M. Cooper, The crystal structure of the ternary alloy α(AlFeSi), Acta Crystall. 23 (6) (1967) 1106–1107.
[3] A. Nicol, The structure of MnAl6, Acta Crystallogr. 6 (1953) 285–293, https://doi.org/10.1107/S0365110X53000788.
[4] D.T.L. Alexander, A.L. Greer, Nucleation of the Al6-to-α-Al—Si transformation in 3XXX aluminium alloys. I. Roll-bonded diffusion couples, Philosophical Magazine, 84(2004) 3051-3070. doi:10.1080/14786430410001701760.
[5] Z.P. Que, Y.P. Zhou, Y. Wang and Z. Fan, Composition Templating for Heterogeneous Nucleation of Intermetallic Compounds, Solidification Processing 2017, 158-161. Conference book.
[6] Aluminium Association: Standard Test Procedure for Aluminium Alloy Grain Refiners: TP-1, Washington DC. 1987.
[7] B.B. Straumal, A.S. Gornakova, Y.O. Kucheev, B. Baretzky, A.N. Nekrasov, Grain boundary Wetting by a Second Solid Phase in the Zr-Nb Alloys, J. Mater. Eng. Perform 21 (5) (2012) 721–724, https://doi.org/10.1007/s11665-012-0158-7.